

Self-Supervised Velocity Estimation for Automotive Radar Object Detection Networks

Daniel Niederlöhner¹, Michael Ulrich², Sascha Braun¹, Daniel Köhler^{1,3}, Florian Faion², Claudius Gläser², André Treptow¹, and Holger Blume³

Abstract—This paper presents a method to learn the Cartesian velocity of objects using an object detection network on automotive radar data. The proposed method is self-supervised in terms of generating its own training signal for the velocities. Labels are only required for single-frame, oriented bounding boxes (OBBs). Labels for the Cartesian velocities or contiguous sequences, which are expensive to obtain, are not required. The general idea is to pre-train an object detection network without velocities using single-frame OBB labels, and then exploit the network’s OBB predictions on unlabelled data for velocity training. In detail, the network’s OBB predictions of the unlabelled frames are updated to the timestamp of a labelled frame using the predicted velocities and the distances between the updated OBBs of the unlabelled frame and the OBB predictions of the labelled frame are used to generate a self-supervised training signal for the velocities. The detection network architecture is extended by a module to account for the temporal relation of multiple scans and a module to represent the radars’ radial velocity measurements explicitly. A two-step approach of first training only OBB detection, followed by training OBB detection and velocities is used. Further, a pre-training with pseudo-labels generated from radar radial velocity measurements bootstraps the self-supervised method of this paper. Experiments on the publicly available nuScenes dataset show that the proposed method almost reaches the velocity estimation performance of a fully supervised training, but does not require expensive velocity labels. Furthermore, we outperform a baseline method which uses only radial velocity measurements as labels.

I. INTRODUCTION

One big challenge in the field of automated driving and advanced driver assistance systems is to perceive and understand the surrounding environment of a vehicle. For this purpose, it is necessary to reliably detect, track and classify all relevant objects. Automotive radar sensors are commonly used beside cameras, ultrasonic sensors and lidar systems. This is due to their low price, robustness in different weather conditions, and ability to measure radial velocities. Furthermore, radar sensors can serve as additional redundancy in highly automated driving. Deep neural networks have shown promising results in solving the object detection tasks for various sensor modalities (e.g. [1], [2], [3]). Object

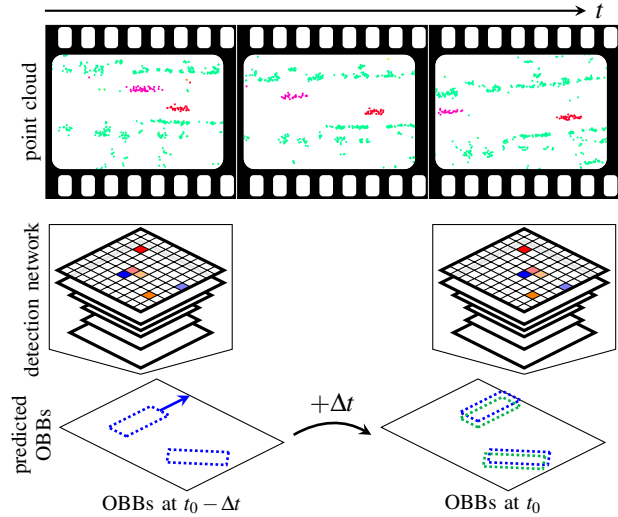


Fig. 1. Velocity estimation in radar object detection networks is important for subsequent tracking. Labelling velocities is expensive, so this paper introduces a self-supervised framework using only oriented bounding box (OBB) labels. Radar point clouds at two timestamps t_0 and $t_0 - \Delta t$ (top row, the color of the points encodes the Doppler velocity) are fed to the network (middle row). The network’s OBB proposals at both timestamps (bottom row) are used for training, where an OBB label exists only for the frame at t_0 . OBB proposals at timestamp $t_0 - \Delta t$ (dashed blue) are first updated to timestamp t_0 using the network’s velocity outputs and afterwards matched with the OBB proposals at timestamp t_0 (solid green) to generate a loss, which serves as a training signal for the predicted velocities. By doing so, our network is able to output OBBs with velocity information without the need of explicit velocity labels.

detection networks are still relatively new for radar, whereas they can already be considered state-of-the-art for image processing [2], [4] and lidar [3], [5]. In recent research, radar data, mainly in the form of spectra or preprocessed point clouds, are used as input to a neural network to solve various problems such as semantic segmentation [6], [7], classification [8], [9], object detection [1], [10], [11], [12], [13] or tracking [14], [15].

To avoid confusion, we define the following terminology in this paper: *Object detection* is used in terms of detecting oriented bounding boxes, as in the deep learning literature and not as *detection* is used in the field of radar signal processing. Further, we use *prediction* to describe the output of a neural network model, in contrast to how the term is used in tracking literature. *Update* denotes the temporal transformation of the position of a bounding box through a motion model, similar to the term *predict* in tracking literature.

¹Sascha Braun, Daniel Köhler, André Treptow and Daniel Niederlöhner are with Robert Bosch GmbH, Cross-Domain Computing Solutions, Germany

²Michael Ulrich, Florian Faion and Claudius Gläser are with Robert Bosch GmbH, Corporate Research, Germany michael.ulrich2@bosch.com

³Daniel Köhler and Holger Blume are with Leibniz University Hannover, Germany

The combination of object detection and tracking is of great importance to obtain a stable environment model from the noisy and sparse radar measurements. Traditional methods typically create objects first and classify the detections afterwards. Deep learning based detection networks perform both tasks simultaneously, overcoming the hand-crafted heuristics required to generate individual objects from multiple radar reflections. These networks usually consume a single scan or multiple time-aggregated scans from one or multiple radar sensors and provide a set of oriented bounding boxes (OBBs) that contain attributes such as class, position, extent, and orientation for all relevant objects in a specific scene. Afterwards, the detections can be tracked for example by using a recursive Bayesian state estimation (e.g. a Kalman Filter) or a tracking network [15], [16], [17] on top of the detector.

The velocity of the objects is of great interest for tracking. Radar sensors can only measure a radial projection of the object’s velocity, i.e. tangential movements to the sensor are not detected. However, the full Cartesian velocity estimates could improve the tracking performance or facilitate track initialization, for instance. Reliable velocity labels are difficult to obtain, in comparison to the above mentioned box attributes because the datasets are usually labelled by humans using lidar and camera data, which do not provide direct velocity information. A common solution is to label the objects position in sequences and estimate the velocity from consecutive frames [15], [18]. Nevertheless, labelling sequences is significantly more expensive than labelling individual frames because many more scenes are required to achieve comparable diversity in the dataset. In this paper, we propose a solution to this problem with the following contributions:

- We propose a radar object detection network that uses point clouds and outputs not only the class, position, extent, and orientation, but also the velocity of objects on a single-shot basis. This network is based on a state-of-the-art architecture [5], for which we introduce extensions to better account for temporal relations and the radar radial velocity measurements.
- We introduce a self-supervised method to learn the full Cartesian velocities. Compared to the Doppler measurement of the radar, this also includes tangential movements to the sensor. Our approach needs only the usual OBB labels to train the detection. Labels for the Cartesian velocity are not required, which reduces the labelling effort significantly.
- We benchmark our algorithms on the publicly available nuScenes dataset [19] and show that we achieve comparable results to a fully supervised velocity regression.

II. RELATED WORK

A. Radar Object Detection

Common approaches often use classical clustering and/or tracking methods to first create object tracks, which are

subsequently classified [8], [20], [21], [22]. In contrast, object detection based approaches simultaneously locate and classify objects using deep neural networks. Such object detection networks can be distinguished by the type of radar input data they consume. Spectrum-based models for object detection utilize 3D radar spectra (range, velocity, azimuth) [23] or reduced 2D [24], [10], [25] or 1D [26], [27] projections.

Other models process radar data in the more abstract form of point clouds, which consist of a list of reflections enhanced with additional features, such as radial velocity v_r and radar cross section σ (RCS). These point cloud based networks can be further differentiated into grid-based and point-based architectures. Grid-based approaches first render the point cloud into a 2D bird eye view (BEV) or 3D voxel grid using hand-crafted operations [11], [28], [29], [30], [31] or learned feature-encoders [32], [12], [31] and subsequently apply convolutional backbones to the grid.

In contrast, point-based methods directly extract features from the radar point cloud without an intermediate grid rendering step. For example [13], [33], [6] adopt PointNet/PointNet++ to achieve a hierarchical feature aggregation of neighbouring points. Other methods in the literature use a graph neural network (GNN) [1], kernel point convolutions [34] or an attention mechanism [35] to exchange contextual information between points.

B. Velocity Estimation

Radar sensors can only measure a radial projection of the object’s velocity which does not contain tangential motion information. Yet, it is possible to calculate the full motion of rigid bodies instantaneously in many cases, using multiple Doppler and azimuth angle measurements. For example, the authors of [36], [37] use the Doppler over azimuth angle profile of multiple reflections on the same object and a RANSAC algorithm to fit the Cartesian velocity. One disadvantage is that these methods need a handcrafted association of points to objects. Deep learning based methods can overcome this bottleneck by learning the association. However, there are only few publications on this topic so far. Often a sensor fusion network is used, that predicts the objects Cartesian velocity components (v_x, v_y) in a vehicle coordinate system as additional box regression attributes. For example, [38] fuses radar and camera data in a CenterNet, while [18] proposes RadarNet, a radar and lidar fusion network which exploits an additional attention-based late fusion step to refine the predicted velocities. With [1] also a radar-only approach has been published. The authors use a GNN for object detection and additionally regress the speed (absolute value of the velocity), assuming that the velocity direction coincides with the box orientation.

Another common method is to use a joint detection and tracking network that processes multiple sequential frames and stores the tracking history internally. The velocities are first predicted by the detection part and filtered afterwards by the tracking network. Such approaches are mostly applied

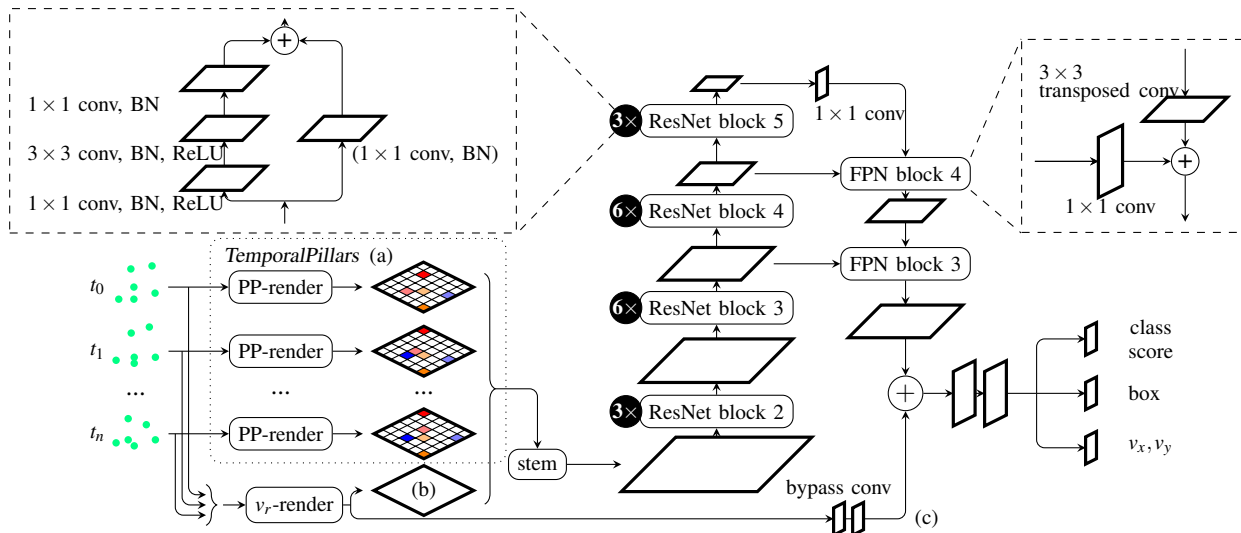


Fig. 2. Architecture of the proposed model. We added: (a) a module *TemporalPillars* to stack feature maps of multiple scans, which are individually processed similar to the PointPillars [32] (PP) rendering, (b) a dedicated feature map for radial velocity measurements (v_r -map) and (c) a shortcut connection of the v_r -map to the detection head. The backbone and the detection head are analogous to [5], with an additional output for the velocity in Cartesian coordinates. $n \times n$ (transposed) conv refers to a 2D (transposed) convolution with kernel size $n \times n$. BN refers to batch normalization.

to lidar (e.g. [16], [17]), but also a first radar-only network has been published [15].

All above approaches require labelled velocities to perform a supervised training. In contrast, the proposed method of this paper learns velocities implicitly and does not require velocity labels.

III. METHOD

A. Overview

This work proposes a radar-only object detection network that outputs 3D bounding boxes with additional Cartesian velocity information without the need of sequence or velocity labels in a self-supervised manner. In this work, self-supervision refers only to the velocity learning and means that all training signals to improve velocity predictions are generated by the network itself on the fly and no explicit velocity or sequence labels are needed. OBB labels are still required, but labels of single frames (non-contiguous time steps) are sufficient.

The core idea is to split the training into two steps, similar to [16]. During the first step (here called *detection step*), the network is trained in a fully supervised way to predict OBBs using 3D box labels and the corresponding radar input data. The velocity output is ignored. In the second step (here called *velocity step*) the network is fed with an unlabelled input, which is close in time to the first step, cf. Fig. 1. The position of the OBB detections are then updated to the timestamp of the *detection step* using the predicted velocities and a fixed (not trainable) constant velocity model. Afterwards, highly confident OBBs of both steps are matched based on the minimal Euclidean distance of the box centers (i.e. OBBs closest to each other are matched). Finally, the distances between the centers of matched boxes are used as a self-supervised loss during backpropagation to train the velocity output. The

constant velocity model is an appropriate choice, as long as the time difference is sufficiently small compared to the objects' dynamics. The two-step approach only affects the network training. During inference, the OBBs and velocities are predicted in a single step.

B. Base Network Architecture

We use a grid-based architecture as depicted in Fig. 2 that processes radar point clouds. First, the reflections are projected onto a BEV grid using a PointPillars-like grid renderer, see [32]. Similar to [31] we found that the grid resolution should be rather coarse ($0.5\text{ m} \times 0.5\text{ m}$), due to the sparsity of radar data. Furthermore, consistently with [31], we found empirically that the backbone and head used in [32] does not perform well with automotive radar data. Instead we adopt the lightweight approach from [5] that uses a 2D convolutional backbone consisting of a residual network [39] and a feature pyramid network [40] to process the BEV feature maps at different resolutions. For a detailed description we refer to [5]. A multitask head predicts both the class scores and the bounding box parameters. In this work we only train the class *car*. Theoretically, other classes can be included in the architecture, but we did not investigate the implications further.

C. Velocity Extension

We added three velocity specific extensions, in addition to the baseline network architecture. We believe that these extensions are easily applicable to a wide range of other radar object detection network architectures:

Velocity output The multitask head is extended with a third output for velocity estimation. This output regresses the Cartesian velocities over ground (v_x, v_y) in the ego vehicle coordinate system by adding another 2D convolutional layer

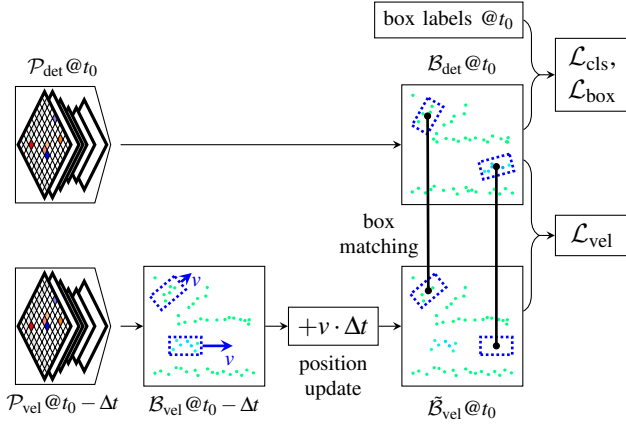


Fig. 3. Scheme of the training process. The networks OBB predictions at two timestamps t_0 and $t_0 - \Delta t$ are used for velocity training. Box positions at timestamp $t_0 - \Delta t$ are updated to t_0 using the predicted velocities and highly confident proposals are matched with boxes from t_0 to obtain a self-supervised loss \mathcal{L}_{vel} . OBB labels at timestamp t_0 are used to calculate the supervised detection losses \mathcal{L}_{cls} and \mathcal{L}_{box} .

with kernel size 3×3 and linear activation. The output directly predicts the v_x and v_y in meters per second without further encoding.

Velocity shortcut In addition, we found that adding the ego motion compensated radial Doppler velocity v_r (without further transformations) to high level feature maps slightly improves the velocity regression. Therefore, we create an additional BEV map (v_r -map) with the same resolution as the PointPillars map, holding the maximum v_r of all radar points within a cell. Empty cells are padded with 0. This v_r -map is concatenated to the output of the PointPillars-like feature maps before the grid is passed to the backbone, cf. Fig. 2(b). Furthermore, there is a shortcut (bypass) path for the radial Doppler information (v_r -map) into high level feature maps, similar to [18]. On this shortcut path, the v_r -map is clipped at ± 50 m/s and normalized. Afterwards, we downsample the v_r -map to the same resolution as the final feature map by applying a 2D convolution with kernel size 3×3 and 16 channels and a bottleneck 2D convolution with kernel size 1×1 and 1 channel, both followed by a max-pooling operation with stride 2. This feature map is then added cell-wise to the feature maps before the head.

TemporalPillars Another change we introduced is a modification to the PointPillars renderer [32]. Radar point clouds are typically quite sparse. It is common practice to increase the density by aggregating multiple consecutive scans [1], [41]. Previous methods from the literature simply used the entire aggregated point cloud $\mathcal{P} = \{\mathcal{P}_1, \dots, \mathcal{P}_n\}$, where n denotes the number of input scans used. In contrast, we feed the point cloud of each scan \mathcal{P}_i (holding all radar sensors) individually into a separate PointPillars renderer and then concatenate all n output maps, to better account for temporal information. The ego vehicle movement is compensated beforehand, such that all scans \mathcal{P}_i refer to a common timestamp. Note that the motion compensation only

works correctly for stationary targets, which is why we add the time difference between the original timestamp of a point and the compensated timestamp as an additional input feature to the network, cf. Sec. III-D. The proposed TemporalPillars is equivalent to the PointPillars renderer for the special case of $n = 1$.

D. Training of the Network

The network is trained using a combination of two different steps: First the fully supervised *detection step* and second the self-supervised *velocity step*. The *velocity step* does not require any labels (self-supervised), while the usual single-snapshot OBB labels are sufficient for the *detection step* (no labelled Cartesian velocity). In both steps, the format of the input point cloud and the network architecture are the same, only training procedure differs. A general overview of the training is shown in Fig. 3.

Detection step In this step, only the box regression and classification part without velocity output is trained in a traditional supervised way with 3D box labels and the corresponding radar input point cloud $\mathcal{P}_{det} = \{p_1, \dots, p_m\}$. The point cloud is a set of m unordered radar reflections $p_i = \{\underline{x}_{p,i}, v_{r,i}, \sigma_i, \alpha_i, \Delta t_i\}$ from all radar sensors from one or multiple temporal aggregated scans, where $\underline{x}_{p,i} \in \mathbb{R}^3$ denotes the ego movement compensated 3D Cartesian position in a common vehicle coordinate system, $v_{r,i} \in \mathbb{R}$ the ego motion compensated radial Doppler velocity, $\sigma_i \in \mathbb{R}$ the radar cross section in dBsm, $\alpha_i \in \mathbb{R}$ the azimuth angle in sensor coordinates and $\Delta t_i \in \mathbb{R}$ the time difference of the measurement to a common reference timestamp of \mathcal{P}_{det} , which is the timestamp of box labels.

The network predicts a set of three dimensional OBB proposals \mathcal{B}_{det} . One OBB $b_i = \{\underline{x}_{c,i}, l_i, w_i, h_i, \theta_i, v_i\}$ is composed of a center position $\underline{x}_{c,i} \in \mathbb{R}^3$ in vehicle coordinates, a length $l_i \in \mathbb{R}$, a width $w_i \in \mathbb{R}$, a height $h_i \in \mathbb{R}$, a yaw orientation angle $\theta_i \in \mathbb{R}$ and a Cartesian velocity vector $v_i = [v_{x,i}, v_{y,i}]^T \in \mathbb{R}^2$ in vehicle coordinates. The roll and pitch angles as well as the velocity in z -direction are omitted. We use the same box encoding as described in [5] for training and decode the box-codes during inference. The velocity output is not encoded and ignored during the *detection step*. For classification we use a focal loss \mathcal{L}_{cls} on all grid cells and for box regression a smooth $L1$ loss \mathcal{L}_{box} only on positive cells (i.e. cells close to a ground truth box). The overall detection loss is composed as a multitask loss $\mathcal{L}_{det} = c_{box}\mathcal{L}_{box} + c_{cls}\mathcal{L}_{cls}$ with the constant weight factors c_{box} and c_{cls} .

Velocity step In the *velocity step*, the network uses an unlabelled point cloud \mathcal{P}_{vel} from a previous frame. We found that a fixed time offset $\Delta t_{vel \rightarrow det} \approx 600$ ms is a suitable value. The point cloud is compensated to the same reference timestamp for both steps (timestamp of \mathcal{P}_{det}), using the movement of the ego vehicle. This means that static points will be located at the same position in both steps. The deviation of the position of dynamic objects is intended to train the velocity predictions, as described in the sequel.

In the forward path, the network produces a set of OBB proposals \mathcal{B}_{vel} from \mathcal{P}_{vel} . The velocity output is trained as follows: First, the proposals are updated to the reference timestamp of \mathcal{P}_{det} by updating the center positions of all boxes in \mathcal{B}_{vel} using a constant velocity model

$$\tilde{x}_{c,i} = x_{c,i} + [v_{x,i}\Delta t_{\text{vel}\rightarrow\text{det}}, v_{y,i}\Delta t_{\text{vel}\rightarrow\text{det}}, 0]^\top \quad (1)$$

while all other box parameters remain unchanged. The updated set of box proposals $\tilde{\mathcal{B}}_{\text{vel}}$ now refers to the same timestamp as the network output from the *detection step*. We keep only highly confident boxes and remove all proposals with a high background classification softmax score $s_{i,\text{bg}}$ of the corresponding box proposal b_i for both *detection step* and updated *velocity step*

$$\tilde{\mathcal{B}}_{\text{vel,conf}} = \{b_i \in \tilde{\mathcal{B}}_{\text{vel}} \mid s_{i,\text{bg}} < \epsilon_{\text{conf}}\} \quad (2)$$

$$\mathcal{B}_{\text{det,conf}} = \{b_i \in \mathcal{B}_{\text{det}} \mid s_{i,\text{bg}} < \epsilon_{\text{conf}}\} \quad (3)$$

where ϵ_{conf} is a constant threshold parameter. A suitable value was derived from the score distributions of all true-positive and false-positive predictions in the dataset, such that there are enough true-positive examples for training while keeping the amount of false-positives sufficiently small. Finally, we match the predictions of both steps by calculating the Euclidean distance $d_{i,j}$ of centers for all box pairs (b_i, b_j) between $\tilde{\mathcal{B}}_{\text{vel,conf}}$ and $\mathcal{B}_{\text{det,conf}}$. The boxes are matched according to the smallest distances and the center distances $d_{i,j}$ of all matches \mathcal{M} are summed to obtain the self-supervised velocity loss

$$\mathcal{L}_{\text{vel}} = \frac{c_{\text{vel}}}{|\mathcal{M}|} \sum_{(i,j) \in \mathcal{M}} d_{i,j} \quad (4)$$

where c_{vel} denotes a constant weight factor and $|\mathcal{M}|$ the number of matches. If the cardinality of $\tilde{\mathcal{B}}_{\text{vel,conf}}$ and $\mathcal{B}_{\text{det,conf}}$ is not equal, we only use $m = \min(|\tilde{\mathcal{B}}_{\text{vel,conf}}|, |\mathcal{B}_{\text{det,conf}}|)$ matches with the smallest Euclidean distance for loss calculation. The velocity output is trained by applying backpropagation to \mathcal{L}_{vel} . We want to highlight, that this step does not incorporate any manual labels.

Training procedure The network is trained in two phases. During the first phase we only apply the supervised *detection step* for several epochs to achieve good detection results. The velocity output is ignored. In the second phase, both steps are performed alternately. Furthermore, our experiments showed that the self-supervised step can be stabilized if the velocity output is pre-trained in the first phase. For this purpose, we use the maximum measured radial Doppler velocity within a ground truth box and project the value to the direction of the box heading. The resulting pseudo labels $(v_{r,x}, v_{r,y})$ are used to train the velocity output by calculating an additional supervised smooth $L1$ loss \mathcal{L}_{vr} which is added to the multitask loss $\mathcal{L}_{\text{det, vr}} = \mathcal{L}_{\text{det}} + c_{\text{vr}}\mathcal{L}_{\text{vr}}$ with a constant weight factor c_{vr} . Note that v_r is only a radial projection of the objects velocity, so the second training phase is still necessary to train the full Cartesian velocity. $(v_{r,x}, v_{r,y})$ are not used during the second training phase.

We conduct our experiments on the publicly available nuScenes dataset [19], which consists of urban real world scenarios recorded in different countries. The evaluation uses the official nuScenes object detection metrics [19] and does not perform radar-specific adjustments, such as removing static objects, filtering the radar field of view, or ignoring boxes without radar points. This makes our results more comparable, even with other modalities. In this work we focus on the *average velocity error* (AVE) to evaluate the quality of the velocity predictions. The AVE is a true-positive metric, meaning that only boxes that match the ground truth are included in the calculation, with a distance threshold of two meters. False-positive detections are not considered in the calculation. It describes the average velocity error between predictions and ground truth boxes in meters per second, see [19]. Further, the detection performance is evaluated in terms of *average precision* at a distance threshold of four meters (AP4.0) and the mean *average precision* of all distance thresholds $\mathbb{D} = \{0.5, 1, 2, 4\}$ meters (AP) per class. We refer to [19] for a more detailed explanation of the metrics.

The hyperparameter were determined empirically. The model is trained for 15 epochs in each of the two training phases using an initial learning rate of 1×10^{-3} in the first phase and 0.5×10^{-3} in the second phase. The constants are set to $c_{\text{cls}} = 10$, $c_{\text{box}} = 0.5$, $c_{\text{vr}} = 0.1$, $c_{\text{vel}} = 0.05$ and $\epsilon_{\text{conf}} = 0.5$. We always use all five radar sensors and augment the input data during training by randomly rotating the entire point cloud in a range of ± 5 degree. Seven consecutive aggregated scans ($\hat{=} 450$ ms for radar sensors in the nuScenes dataset) of radar data are used per frame. All evaluations are performed on the official nuScenes validation split. The ground truth values for the velocity are derived based on the position change in sequential frames. We only train on class *car*. Other classes are possible, but for radar the detection performance is typically worse, due to the sparsity of the point cloud and the class imbalance in the dataset. This might affect the self-supervised *velocity step* negatively.

For lack of previous published work, we conduct a supervised training of velocities as an error lower bound. Furthermore, we compare our method against a supervised training that only uses the maximum measured radial Doppler velocity within a ground truth box projected to the direction of the box heading $(v_{r,x}, v_{r,y})$ as labels. Both supervised approaches are trained for 15 epochs without applying the *velocity step* (i.e. only the first training phase is used).

The results are summarized in Tab. I. It can be observed, that the proposed method achieves a lower AVE than the training with projected Doppler velocities and almost reaches the performance bound of the supervised velocity vector training. The AVE averages over all true positives, where many samples are simple stationary objects or longitudinally moving traffic. The Cartesian velocities in such cases are already well predicted by the projected Doppler approach. Hence, an AVE improvement of 0.065 m/s is quite signif-

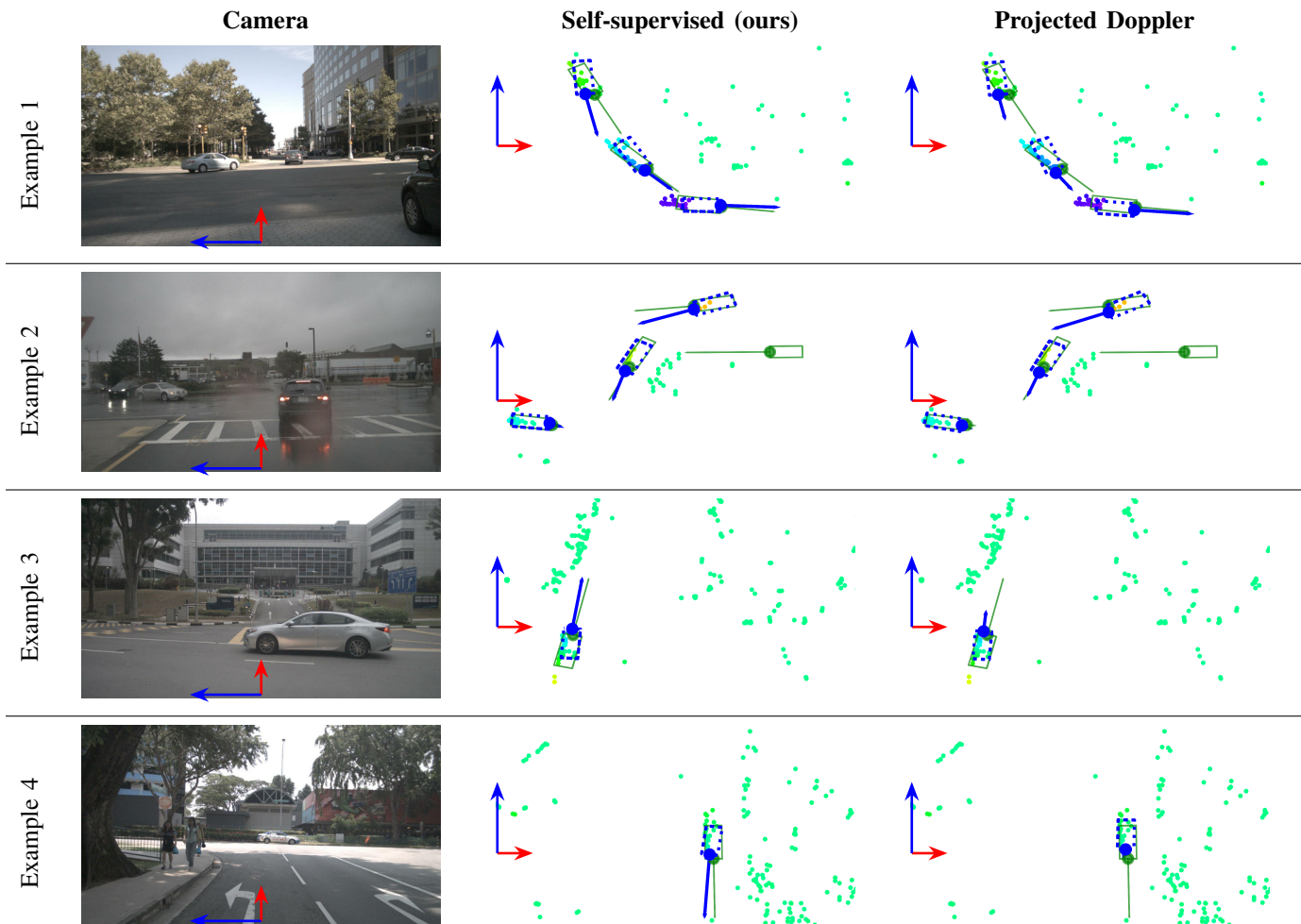


Fig. 4. Camera images and a bird eye view plot of the radar point clouds and network outputs of our self-supervised approach vs. the projected Doppler lower performance boundary in different nuScenes samples. Radar reflections are represented as colored dots. The color encodes the ego motion compensated Doppler velocity, where green corresponds to no radial motion. Predicted boxes are drawn with dashed blue lines \square and ground truth boxes with solid green lines \square . The velocities are drawn as oriented arrows with a length proportional to the absolute speed in the same color as the boxes. It can be seen that our self-supervised training significantly outperforms the Doppler approach for tangential motions to the radar sensor (see velocity differences in Example 3 and 4), while there is almost no difference between the two approaches for radial movements (see longitudinal objects in Example 1 and 2). Furthermore, in Example 2 there is a ground truth box that could not be detected due to a lack of radar measurements.

TABLE I

BENCHMARK OF OUR NETWORK USING DIFFERENT VELOCITY TARGETS EVALUATED ON THE NUSCENES VALIDATION DATASET FOR CLASS *car*

Velocity target	requires OBB labels	requires velocity labels	AP (%) \uparrow	AP4.0 (%) \uparrow	AVE (m/s) \downarrow
label	yes	yes	23.47	38.45	0.480
self-supervised (ours)	yes	no	23.49	39.03	0.515
projected Doppler	yes	no	23.86	39.29	0.580

TABLE II

ABLATION STUDY: IMPACT OF DIFFERENT NETWORK EXTENSIONS
EVALUATED ON THE NUSCENES VALIDATION DATASET FOR CLASS *car*

Network configuration	AP (%) \uparrow	AP4.0 (%) \uparrow	AVE (m/s) \downarrow
no v_r pre-training	22.31	38.36	0.797
no TemporalPillars	22.18	37.55	0.561
no v_r -map	23.23	38.71	0.541
Proposed (ours)	23.49	39.03	0.515

TABLE III

ABLATION STUDY: DIFFERENT NUMBER OF AGGREGATED SCANS
EVALUATED ON THE NUSCENES VALIDATION DATASET FOR CLASS *car*

Number of scans	AP (%) \uparrow	AP4.0 (%) \uparrow	AVE (m/s) \downarrow
1	14.67	27.93	0.727
3	19.77	34.67	0.638
5	22.25	37.53	0.600
7	23.49	39.03	0.515

icant, considering that a large gain is only achievable for a small number of OBBs.

Examples are shown in Fig. 4, where the approach using the projected Doppler fails predicting the velocities of tangentially moving objects, while the presented self-supervised approach can handle the scenarios, even in difficult situations such as roundabouts or at intersections. However, our model sometimes tends to predict an inaccurate velocity estimate (direction and absolute value) when only a few radar points are measured on an object, cf. Fig. 4 (Example 1 and 2). This is probably due to the low information density and the high position variance typical for radar measurements. The detection performance of the three methods is similar, as expected. The AP and AP4.0 is slightly better for the projected Doppler-based training, where the proposed methods marginally outperforms the fully supervised training. However, the difference in detection performance is not significant.

In addition, we conducted ablation studies to investigate the impact of the network extensions described in Sec. III-C and Sec. III-D as well as the impact of the number of scans aggregated in the input point cloud. The results for different configurations are shown in Tab. II, where *Proposed* refers to the self-supervised approach as described in this paper. In this experiment, single components are omitted, i.e. the Doppler-based pre-training, the TemporalPillars and the v_r -map. The results show that the Doppler-based pre-training has a high impact on the velocity estimation. Clearly, the network architecture is the same with and without this pre-training, but training convergence is highly affected. We have observed that \mathcal{L}_{vel} can be quite noisy, which makes a good initialization of the network weights necessary. Next, the use of TemporalPillars reduces the velocity error by roughly 8%, in comparison to merging all scans in a single point cloud. Further, we observe that the TemporalPillars also improves the detection performance. Similarly, the proposed v_r -map as input to the backbone and through the shortcut improved the velocity estimation.

A second ablation study investigates the impact of the number of radar scans which are aggregated in one frame in Tab. III. We aggregated 1, 3, 5 and 7 scans, corresponding to a time interval of 0 ms, 150 ms, 300 ms and 450 ms, respectively, for the nuScenes radar sensors. Obviously, a larger aggregation interval improves both detection performance and velocity estimates, but also introduces more delay and temporal correlation in a subsequent tracking system. In addition, the shape and position information of objects can be distorted, especially if they are moving. Interestingly, the reduction from 7 to 5 scans increases the velocity error significantly. We believe that this might be because the radar point reflections on the vehicles are not at consistent places but at random locations on the car. A short history (trace) might not be sufficient to observe the overall trend in which direction the object is moving. Furthermore, it can be observed that velocity estimation is also possible with a single scan. Clearly, the history (trace) of reflection points

improves the performance, but usable information is also present in the radial velocity measurements.

V. CONCLUSION

In this paper, we presented a self-supervised velocity regression approach for single-shot radar object detection networks and proposed a suitable network architecture. The training consists of two parts: A supervised box detection part and a self-supervised velocity regression part. A combination of both parts results in a network capable of predicting oriented bounding boxes and corresponding Cartesian velocities without the need for sequence or velocity labels. Our experiments on the publicly available nuScenes dataset showed that our method can achieve comparable results to a fully supervised training. The proposed approach is particularly useful when velocity labels are not available. Labels for Cartesian velocity would be expensive to obtain, but are not required by the proposed method. Possible extensions of this work could use the proposed self-supervised velocity estimation for pre-training or as an auxiliary task. In addition, motion models other than the constant velocity model could be tested and the time interval between *detection step* and *velocity step* $\Delta t_{vel \rightarrow det}$ could be varied during training, which might increase the robustness of the velocity estimate.

REFERENCES

- [1] P. Svenningsson, F. Fioranelli, and A. Yarovoy, "Radar-PointGNN: Graph based object recognition for unstructured radar point-cloud data," in *2021 IEEE Radar Conference*, pp. 1–6, May 2021. ISSN: 2375-5318.
- [2] W. Liu, D. Anguelov, D. Erhan, C. Szegedy, S. Reed, C.-Y. Fu, and A. C. Berg, "SSD: Single shot multibox detector," in *Computer Vision – ECCV 2016*, Lecture Notes in Computer Science, pp. 21–37, Springer International Publishing, 2016.
- [3] Y. Zhou and O. Tuzel, "VoxelNet: End-to-end learning for point cloud based 3D object detection," *arXiv:1711.06396 [cs]*, Nov. 2017. arXiv: 1711.06396.
- [4] K. He, G. Gkioxari, P. Dollár, and R. Girshick, "Mask R-CNN," in *2017 IEEE International Conference on Computer Vision (ICCV)*, pp. 2980–2988, Oct. 2017. ISSN: 2380-7504.
- [5] B. Yang, W. Luo, and R. Urtasun, "PIXOR: Real-time 3D object detection from point clouds," *arXiv:1902.06326 [cs]*, Mar. 2019. arXiv: 1902.06326.
- [6] O. Schumann, J. Lombacher, M. Hahn, C. Wöhler, and J. Dickmann, "Scene understanding with automotive radar," *IEEE Transactions on Intelligent Vehicles*, vol. 5, no. 2, pp. 188–203, 2020.
- [7] A. Ouaknine, A. Newson, P. Pérez, F. Tupin, and J. Rebut, "Multi-view radar semantic segmentation," in *Proceedings of the IEEE/CVF International Conference on Computer Vision (ICCV)*, pp. 15671–15680, October 2021.
- [8] M. Ulrich, C. Gläser, and F. Timm, "DeepReflects: Deep learning for automotive object classification with radar reflections," in *2021 IEEE Radar Conference (RadarConf21)*, pp. 1–6, IEEE, 2021.
- [9] K. Patel, K. Rambach, T. Visentin, D. Rusev, M. Pfeiffer, and B. Yang, "Deep learning-based object classification on automotive radar spectra," in *2019 IEEE Radar Conference (RadarConf)*, pp. 1–6, 2019.
- [10] Y. Wang, Z. Jiang, X. Gao, J.-N. Hwang, G. Xing, and H. Liu, "RODNet: Radar object detection using cross-modal supervision," in *Proceedings of the IEEE/CVF Winter Conference on Applications of Computer Vision*, pp. 504–513, 2021.
- [11] M. Dreher, E. Erçelik, T. Bänziger, and A. Knol, "Radar-based 2D car detection using deep neural networks," in *2020 IEEE 23rd International Conference on Intelligent Transportation Systems (ITSC)*, pp. 1–8, IEEE, 2020.

- [12] B. Xu, X. Zhang, L. Wang, X. Hu, Z. Li, S. Pan, J. Li, and Y. Deng, "RPFA-Net: A 4D radar pillar feature attention network for 3D object detection," in *2021 IEEE International Intelligent Transportation Systems Conference (ITSC)*, pp. 3061–3066, Sept. 2021.
- [13] A. Danzer, T. Griebel, M. Bach, and K. Dietmayer, "2D car detection in radar data with PointNets," *2019 IEEE Intelligent Transportation Systems Conference (ITSC)*, pp. 61–66, Oct. 2019. arXiv: 1904.08414.
- [14] J. Ebert, T. Gumpff, S. Münzner, A. Matskevych, A. P. Condurache, and C. Gläser, "Deep radar sensor models for accurate and robust object tracking," in *2020 IEEE 23rd International Conference on Intelligent Transportation Systems (ITSC)*, pp. 1–6, IEEE, 2020.
- [15] J. F. Tilly, S. Haag, O. Schumann, F. Weishaupt, B. Duraisamy, J. Dickmann, and M. Fritzsche, "Detection and tracking on automotive radar data with deep learning," in *2020 IEEE 23rd International Conference on Information Fusion (FUSION)*, pp. 1–7, 2020.
- [16] T. Yin, X. Zhou, and P. Krähennühl, "Center-based 3D object detection and tracking," *arXiv:2006.11275 [cs]*, Jan. 2021. arXiv: 2006.11275.
- [17] W. Luo, B. Yang, and R. Urtasun, "Fast and Furious: Real time end-to-end 3D detection, tracking and motion forecasting with a single convolutional net," *CoRR*, vol. abs/2012.12395, 2020.
- [18] B. Yang, R. Guo, M. Liang, S. Casas, and R. Urtasun, "RadarNet: Exploiting radar for robust perception of dynamic objects," in *Computer Vision – ECCV 2020*, pp. 496–512, 2020.
- [19] H. Caesar, V. Bankiti, A. H. Lang, S. Vora, V. E. Liong, Q. Xu, A. Krishnan, Y. Pan, G. Baldan, and O. Beijbom, "nuScenes: A multimodal dataset for autonomous driving," in *Proceedings of the IEEE/CVF conference on computer vision and pattern recognition*, pp. 11621–11631, 2020.
- [20] O. Schumann, C. Wöhler, M. Hahn, and J. Dickmann, "Comparison of random forest and long short-term memory network performances in classification tasks using radar," in *2017 Sensor Data Fusion: Trends, Solutions, Applications (SDF)*, pp. 1–6, 2017.
- [21] O. Schumann, M. Hahn, J. Dickmann, and C. Wöhler, "Supervised clustering for radar applications: On the way to radar instance segmentation," in *2018 IEEE MTT-S International Conference on Microwaves for Intelligent Mobility (ICMIM)*, pp. 1–4, 2018.
- [22] N. Scheiner, O. Schumann, F. Kraus, N. Appenrodt, J. Dickmann, and B. Sick, "Off-the-shelf sensor vs. experimental radar-how much resolution is necessary in automotive radar classification?," in *2020 IEEE 23rd International Conference on Information Fusion (FUSION)*, pp. 1–8, IEEE, 2020.
- [23] A. Palffy, J. Dong, J. F. Kooij, and D. M. Gavrila, "CNN based road user detection using the 3D radar cube," *IEEE Robotics and Automation Letters*, vol. 5, no. 2, pp. 1263–1270, 2020.
- [24] D. Brodeski, I. Bilik, and R. Giryes, "Deep radar detector," in *2019 IEEE Radar Conference (RadarConf)*, pp. 1–6, Apr. 2019. ISSN: 2375-5318.
- [25] M. Meyer, G. Kuschik, and S. Tomforde, "Graph convolutional networks for 3D object detection on radar data," in *2021 IEEE/CVF International Conference on Computer Vision Workshops (ICCVW)*, pp. 3053–3062, 2021.
- [26] M. Ulrich, T. Hess, S. Abdulatif, and B. Yang, "Person recognition based on micro-Doppler and thermal infrared camera fusion for firefighting," in *2018 21st International Conference on Information Fusion (FUSION)*, pp. 919–926, 2018.
- [27] M. Ulrich and B. Yang, "Short-duration Doppler spectrogram for person recognition with a handheld radar," in *2018 26th European Signal Processing Conference (EUSIPCO)*, pp. 1227–1231, 2018.
- [28] F. Nobis, E. Shafei, P. Karle, J. Betz, and M. Lienkamp, "Radar voxel fusion for 3D object detection," *Applied Sciences*, vol. 11, p. 5598, Jan. 2021.
- [29] S. Lee, "Deep learning on radar centric 3D object detection," *arXiv:2003.00851 [cs, eess]*, Feb. 2020. arXiv: 2003.00851.
- [30] M. Meyer and G. Kuschik, "Deep learning based 3D object detection for automotive radar and camera," in *2019 16th European Radar Conference (EuRAD)*, pp. 133–136, 2019.
- [31] N. Scheiner, F. Kraus, N. Appenrodt, J. Dickmann, and B. Sick, "Object detection for automotive radar point clouds - a comparison," *AI Perspectives*, vol. 3, p. 6, Nov. 2021.
- [32] A. H. Lang, S. Vora, H. Caesar, L. Zhou, J. Yang, and O. Beijbom, "PointPillars: Fast encoders for object detection from point clouds," in *Proceedings of the IEEE/CVF Conference on Computer Vision and Pattern Recognition*, pp. 12697–12705, 2019.
- [33] K. Bansal, K. Rungta, S. Zhu, and D. Bharadia, "Pointillism: Accurate 3D bounding box estimation with multi-radars," *SenSys*, 2020.
- [34] F. Nobis, F. Fent, J. Betz, and M. Lienkamp, "Kernel point convolution LSTM networks for radar point cloud segmentation," *Applied Sciences*, vol. 11, p. 2599, Jan. 2021.
- [35] J. Bai, L. Zheng, S. Li, B. Tan, S. Chen, and L. Huang, "Radar transformer: An object classification network based on 4D MMW imaging radar," *Sensors*, vol. 21, no. 11, p. 3854, 2021.
- [36] D. Kellner, M. Barjenbruch, K. Dietmayer, J. Klappstein, and J. Dickmann, "Instantaneous lateral velocity estimation of a vehicle using Doppler radar," in *Proceedings of the 16th International Conference on Information Fusion*, pp. 877–884, 2013.
- [37] D. Kellner, M. Barjenbruch, J. Klappstein, J. Dickmann, and K. Dietmayer, "Instantaneous full-motion estimation of arbitrary objects using dual Doppler radar," in *2014 IEEE Intelligent Vehicles Symposium Proceedings*, pp. 324–329, 2014.
- [38] R. Nabati and H. Qi, "Centerfusion: Center-based radar and camera fusion for 3D object detection," in *2021 IEEE Winter Conference on Applications of Computer Vision (WACV)*, pp. 1526–1535, 2021.
- [39] K. He, X. Zhang, S. Ren, and J. Sun, "Deep residual learning for image recognition," in *2016 IEEE Conference on Computer Vision and Pattern Recognition (CVPR)*, pp. 770–778, June 2016. ISSN: 1063-6919.
- [40] T.-Y. Lin, P. Dollár, R. Girshick, K. He, B. Hariharan, and S. Belongie, "Feature pyramid networks for object detection," *arXiv:1612.03144 [cs]*, Apr. 2017. arXiv: 1612.03144.
- [41] L. Wang, T. Chen, C. Anklam, and B. Goldluecke, "High dimensional frustum PointNet for 3D object detection from camera, lidar, and radar," in *2020 IEEE Intelligent Vehicles Symposium (IV)*, pp. 1621–1628, 2020.